JCTC Journal of Chemical Theory and Computation

CBS-QB3 + VTST Study of Methyl *N*-Methylcarbamate + OH Gas-Phase Reaction: Mechanism, Kinetics, and Branching Ratios

Claudia Zavala-Oseguera[†] and Annia Galano*[,‡]

Departamento de Química, Universidad de Guanajuato, Noria Alta s/n C.P. 36050, Guanajuato, Gto. México, and Departamento de Química, Universidad Autónoma Metropolitana-Iztapalapa, San Rafael Atlixco 186, Col. Vicentina, Iztapalapa, C.P. 09340, México, D. F. México

Received February 4, 2009

Abstract: Different paths of reaction have been modeled, at high level of theory, accounting for the possible atmospheric fate of methyl *N*-methylcarbamate (MMC). The OH hydrogen abstractions from the methyl groups are predicted to account for almost 100% of the MMC + OH gas-phase reaction. The H abstraction from the methyl group at the N side of MMC was found to be the main path of reaction, with contributions to the overall reaction from 96% at 260 K to 89.2% at 400 K. Hydrogen abstractions from the other methyl group were identified as a secondary, but significant path. The Arrhenius activation energy, in the temperature range 260−400 K, was found to be close to zero, but slightly negative. The proposed value is (−0.10 ± 0.02) kcal/mol. The excellent agreement with the scarce experimental data available supports the reliability of the data reported here for the first time. Different IVTST-M-*H*/*G* schemes were tested for dynamic calculations. According to our results, including the Hessians and gradients, as few as four nonstationary points along the MEP is sufficient to achieve an excellent accuracy, provided that the data for these few points were obtained from high-quality levels of theory.

Introduction

Carbamates are versatile organic compounds with a wide range of applications. They are used as agrochemical agents with pesticide, fungicide, and herbicide activities.[1−4] They are also used as drug intermediates in the pharmaceuticals industry,[1,2,5] and in the polymer industry in the synthesis of polyurethane[1,2] and also in peptide syntheses.[5] In addition, among the various amine-protecting groups, carbamates are commonly used due to their chemical stability toward acids, bases, and hydrogenation.[6] Their general formula is $R_1N(H)C(O)OR_2$, where R_1 and R_2 can be alkyl or aryl groups.

Numerous studies have been devoted to the synthesis of carbamates; however, there is very scarce information of their fate after they are released into the environment. Carbamates with low molecular weights are volatile organic compounds (VOCs), and as for any other VOC their reaction with OH radicals is expected to be an important, or even the dominant, atmospheric loss process.[7,8]

Methyl *N*-methylcarbamate (MMC) is the simplest of this broad class of compounds, and that is why it has been selected for the present study. In an early work by Daly and Ziolkowski,[9] MMC was found to unimolecularly decompose in the gas phase, yielding methyl isocyanate and methanol in the temperature range 370−422 K. The mechanistic pathway of this reaction was explained in terms of a four-membered cyclic transition state. However, no further studies have been conducted in this direction.

In a recent work, Kwok et al.[10] reported the rate constants of OH gas-phase reactions with four alkyl carbamates at (296 ± 2) K. For MMC, the reported value is $(4.3 \pm 1.2) \times 10^{-12}$ cm^3 $molecule^{-1}$ s^{-1}. They proposed,[10] by analogy with thiocarbamates,[11] that the OH radical reactions with carbamates are expected to proceed by H-atom abstraction from

* Corresponding author e-mail: agalano@prodigy.net.mx.
[†] Universidad de Guanajuato.
[‡] Universidad Autónoma Metropolitana-Iztapalapa.

10.1021/ct9000679 CCC: $40.75 © 2009 American Chemical Society
Published on Web 04/17/2009

the C−H bonds of the alkyl substituent groups and by initial addition to the N atom of the −N(H)C(O)O− moiety. They also found that the measured rate constants for the carbamates increase by replacing a methyl group by an ethyl group on both the ester site and the N atom. However, this increase is larger for the latter (2.4 vs 1.9 times larger). From these results, it can be inferred that if similar alkyl groups are bonded to the N and the O atoms, the contribution of H abstraction from the alkyl group on the N atom should be larger than that of the alkyl group on the ester group.

However, to our best knowledge, there is no available information on the branching ratios of these reactions. Actually, there is scarce information on branching ratios for VOCs reactions in general. Therefore, further efforts in this direction are needed since it has been established that branching ratios between different products in multichanneled reactions are as important as the overall rate of reaction, in terms of practical applications and in the understanding of the fundamental mechanisms of chemical reactions.[12−15]

In view of the above exposed arguments, the principal aim of this work is to model the different reactive pathways of the OH reactions with MMC and to estimate the proportion of their contribution to the overall reactions. For that purpose, the mechanism and the kinetics of this reaction have been studied as accurately as possible, using CBS-QB3 methodology for energies and variational transition state theory (VTST) for rate constants. In addition, a study of the temperature dependence of the rate coefficients was performed over the temperature range 260−400 K, and kinetic parameters are proposed for the first time.

Computational Details

All of the electronic structure calculations have been performed with the Gaussian 03 package of programs.[16] The high-level composite method CBS-QB3[17] has been used for all of the calculations. The complete basis set (CBS) models are compound methods that extrapolate to the CBS limit by using a $N - 1$ asymptotic convergence of MP2 pair energies calculated from pair natural orbital expansions.[17,18] They were developed to overcome the truncation of the basis sets, which is a major source of error in quantum mechanical calculations. CBS-QB3 is a five-step method that starts with B3LYP geometry and frequency calculations, followed by CCSD(T), MP4SDQ, and MP2 single-point calculations and a CBS extrapolation.[17] It also corrects for spin contamination.

Local minima and transition states were identified by the number of imaginary frequencies (NIMAG = 0 or 1, respectively). Intrinsic reaction coordinate (IRC)[19] calculations were carried out at B3LYP/CBSB7 level of theory to confirm that the transition states structures connect the proper reactants and products. The paths have been computed by following the Gonzalez−Schlegel steepest descent path,[20] in mass-weighted internal coordinates. Twenty points were modeled on each side of the saddle points, with a gradient step size of 0.05 amu$^{1/2}$ bohr. Thermodynamic corrections to the energy at 298.15 K were included in the determination of the energy barriers and of the heats of reaction, which have been reported in terms of Gibbs free energies.

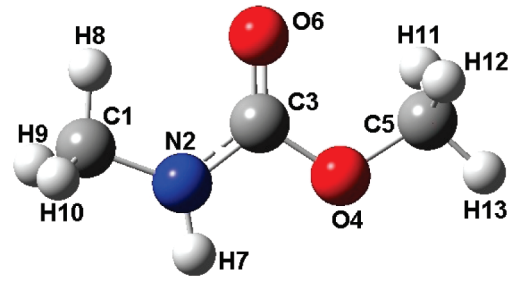

Figure 1. Atom numbering for methyl *N*-methylcarbamate.

The rate constant calculations for H abstraction paths were carried out by direct dynamics with the Interpolated Variational Transition-State Theory by Mapping (IVTST-M),[21] as implemented in POLYRATE 9.1.[22] In the IVTST-M algorithm, the calculations of rate constants evaluated by Canonical Variational Theory (CVT)[23] with Small-Curvature Tunneling (SCT) corrections are based on reaction-path data. The energies, energy gradients, and Hessians are computed at a small number of points along the minimum energy path (MEP) and fitted to splines under tension as functions of a mapped independent variable that is a nonlinear function of the reaction coordinate.[21] The notation IVTST-M-*H*/*G* means that interpolations are based on optimized calculations of stationary points (reactants, reactant complex, transition state, product complex, and product) plus *G* additional energies and gradients, and *H* additional Hessians corresponding to nonstationary points on the MEP. The different levels for dynamic calculations tested in this work are IVTST-M-8/10, IVTST-M-8/8, IVTST-M-6/8, IVTST-M-6/6, IVTST-M-4/10, IVTST-M-4/8, IVTST-M-4/6, IVTST-M-4/4, IVTST-M-2/4, and IVTST-M-2/2. All of the dynamic calculations in the present Article employ redundant internal coordinates for generalized normal-mode analyses.[25] We have used a step size of $0.01a_0$ for all IVTST-M calculations. The additional points on the MEP were chosen at a distance of $s = \pm 0.1$, 0.2, 0.4, and 0.6 amu$^{1/2}$ a_0 from the saddle point, where s represents the intrinsic reaction coordinate.

For OH addition and unimolecular fragmentation, the Conventional Transition State Theory (TST)[26] was used because the corresponding reaction barriers are high enough to safely assume that the variational effects are negligible. Tunneling factors were computed, in these cases, assuming an unsymmetrical, one-dimensional, Eckart function barrier.[27]

Results and Discussion

Structures and Energies. The optimized structure of MMC is shown in Figure 1, together with the atom numbering used through this Article. The atoms in the hydroxyl radical have been labeled as 14 and 15, referring to O and H atoms, respectively.

Seven different decomposition pathways related to MMC fate after it is released into the environment have been modeled.

Path I represents the unimolecular fragmentation proposed by Daly and Ziolkowski,[9] leading to the formation of methyl isocyanate and methanol:

$$CH_3N(H)C(O)OCH_3 \rightarrow CH_3NCO + CH_3OH \qquad (I)$$

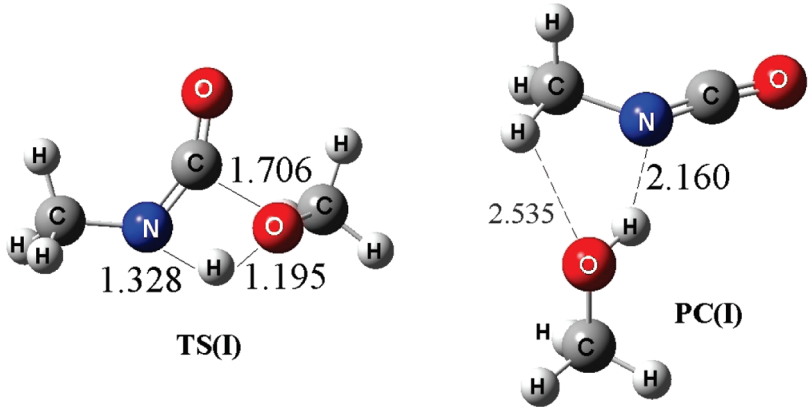

Figure 2. Optimized geometries of the transition state and product complex from path I.

A four-membered transition state (TS), consistent with the mechanism proposed by the above-mentioned authors, has been located for this path (Figure 2). It corresponds to a concerted mechanism with the breaking of C3−O4 and N2−H7 bonds and the formation of the O4−H7 bond occurring simultaneously. The bond distances d_{C3O4} and d_{N2H7} were found to be 0.344 and 0.321 Å larger in the TS than in MMC. The bond angles (a) in the four-membered ring have values of $a_{N2C3O4} = 90.4°$, $a_{C3O4H7} = 70.4°$, $a_{O4H7N2} = 116.8°$, and $a_{H7N2C3} = 82.2°$. While in MMC all non-hydrogen atoms are located on a plane, the dihedral/torsion angle is $t_{C5O4C3N2} = 118.9°$ in TS(I). A weak bonded complex has been identified in the product channel (Figure 2) with the main interaction involving the hydroxylic H in methanol and the N atom in methyl isocyanate. A secondary interaction was also found, between the O atom in methanol and one of the H atoms in methyl isocyanate.

The above-described transition state is 53.0 and 52.9 kcal/mol higher than the reactant, in terms of Gibbs free energy and enthalpy, respectively. This path was found to be endothermic and endergonic with $\Delta H_I = 24.5$, and $\Delta G_I = 12.5$ kcal/mol, at 298.15 K. According to these results, path I is not expected to significantly contribute to the overall environmental evolution of MMC.

Paths II, III, and IV account for OH hydrogen abstraction reactions from MMC. Paths II and IV represent H-atom abstraction from the methyl groups, as proposed by Kwok et al.,[10] while path III represents H abstraction from the NH group:

$$CH_3N(H)C(O)OCH_3 + {}^{\bullet}OH \rightarrow CH_3N(H)C(O)O{}^{\bullet}CH_2 + H_2O \quad \text{(II)}$$

$$\rightarrow CH_3N{}^{\bullet}C(O)OCH_3 + H_2O \quad \text{(III)}$$

$$\rightarrow {}^{\bullet}CH_2N(H)C(O)OCH_3 + H_2O \quad \text{(IV)}$$

Reactant complexes (RC) and product complexes (PC) were found for all of the abstraction paths in the entrance and exit channels, respectively (Figure 3). All of them show ring-like structures, caused by two interactions. In the RCs, the strongest interaction always involves the H atom in the hydroxyl radical and one of the O atoms in MMC. The secondary interaction involves the O in the OH radical and an H atom in the methyl (paths II and IV) or in the amide (path III) groups. In the PCs, the strongest interaction involves one H atom in the water fragment and one of the O atoms in the MMC formed radicals, while the secondary interaction involves the other H in water and the radical center in MMC radicals.

In all of the transition states, intramolecular H bonds were found between the H atom in the hydroxyl radical and one of the O atoms in MMC. This stabilizing interaction was found to be the strongest for TS(II) with the interaction distance $d'_{O6H14} = 2.186$ Å, followed by TS(IV) and TS(III), in that order, with d'_{O6H14} and d'_{O4H14} equal to 2.247 and 2.466 Å, respectively. The major structural changes in transition states II and IV, as compared to MMC, are the elongation of the C−H bond by 0.119 and 0.088 Å, respectively, and the shortening of the C−O and C−N distances by 0.025 and 0.019 Å. For TS(III), the main structural difference with respect to MMC is the elongation of the N−H distance by 0.155 Å.

All of the abstraction paths were found to be exothermic and exergonic with $\Delta H_{II} = -19.23$, $\Delta H_{III} = -10.9$, $\Delta H_{IV} = -24.5$, $\Delta G_{II} = -20.4$, $\Delta G_{III} = -11.6$, and $\Delta G_{IV} = -25.7$ kcal/mol, at 298.15 K. Accordingly, path IV is the most thermodynamically favored, while path III is the least favored, among the H abstraction channels. The barriers of reactions, in terms of Gibbs free energy, were found to be $\Delta G^{\ddagger}_{II} = 8.0$, $\Delta G^{\ddagger}_{III} = 11.0$, and $\Delta G^{\ddagger}_{IV} = 7.4$ kcal/mol. On the basis of these results, it is expected that H abstraction reactions mainly involve the methyl groups in MMC, and especially the one in the amidic end.

Three different pathways have been tested for OH addition reactions to MMC. Path V represents the OH addition to the N atom in the −N(H)C(O)O− moiety as proposed by Kwok et al.,[10] while paths VI and VII represent OH additions to the C and O atoms in the carbonyl group, respectively:

$$CH_3N(H)C(O)OCH_3 + {}^{\bullet}OH \rightarrow CH_3{}^{\bullet}N(H,OH)C(O)OCH_3 \quad \text{(V)}$$

$$\rightarrow CH_3N(H){}^{\bullet}C(O,OH)OCH_3 \quad \text{(VI)}$$

$$\rightarrow CH_3NHC{}^{\bullet}(O-OH)OCH_3 \quad \text{(VII)}$$

Any attempt to locate the products of additions V and VII invariably led to the separation into the reactant fragments. Product V evolves toward RC(III) structure, and product VII

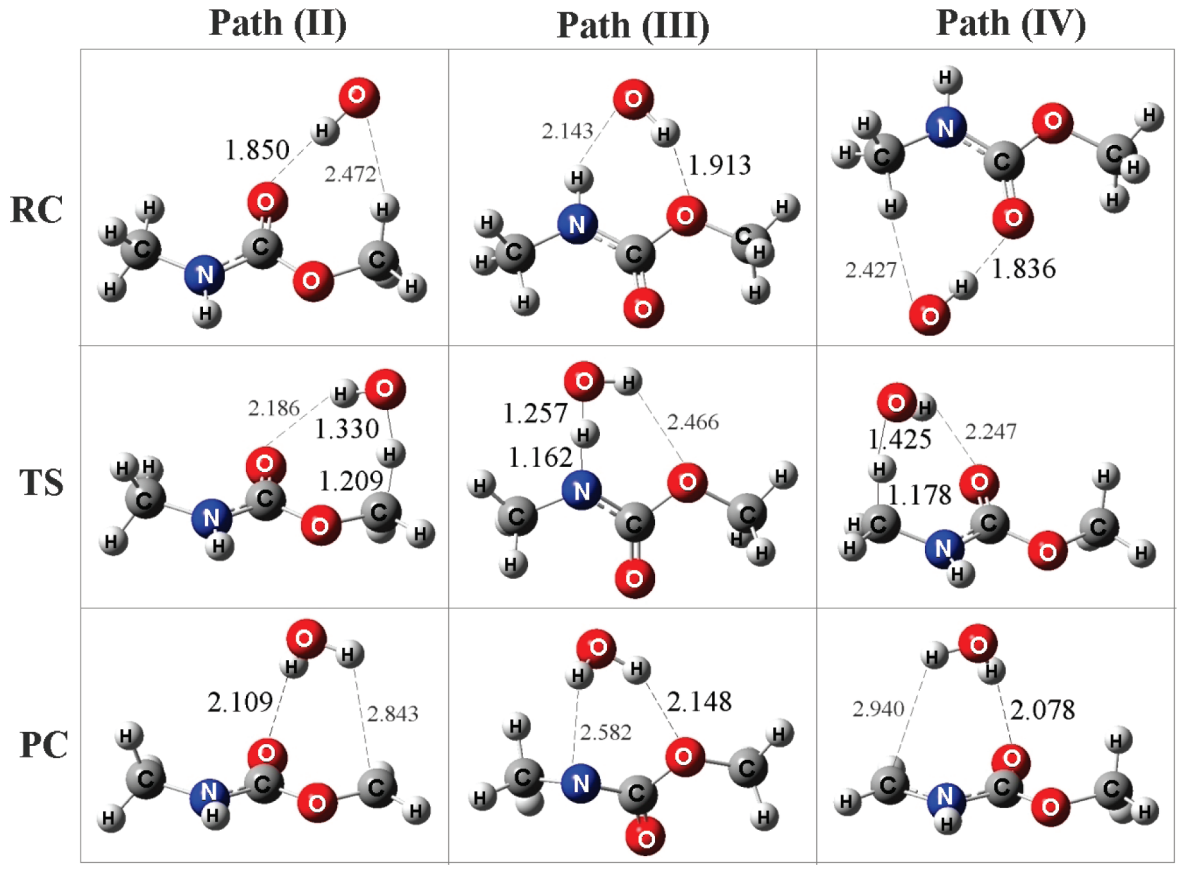

Figure 3. Optimized geometries of reactant complexes (RC), transition states (TS), and product complexes (PC) from paths II, III, and IV.

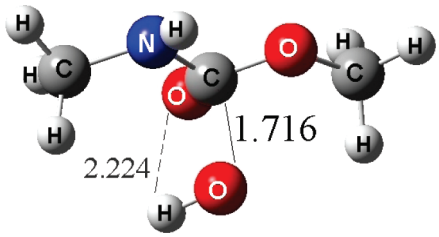

Figure 4. Optimized geometry of the transition state from path VI.

toward RC(II). Accordingly, the OH additions to the N atom of the −N(H)C(=O)O− moiety and to the O atom in the carbonyl group have been ruled out. For path VI, the addition product was located with C3 in tetrahedral configuration and d_{C3O14} = 1.408 Å, which corresponds to the newly formed C−O bond. A reactant complex was found in the entrance channel, and it is identical to RC(II). The structure shows a ring-like structure, with an intramolecular interaction between O6 in MMC and the H atom in the OH radical. The main structural changes, as compared to free MMC, are the elongation of the C3−O6 and C3−N2 bonds, by 0.085 and 0.023 Å, respectively.

Path VI (Figure 4) was found to be slightly exothermic and significantly endergonic, with $\Delta H_{VI} = -0.1$, $\Delta G_{VI} =$ 11.3 kcal/mol. The calculated barrier height is 22.8 kcal/mol in terms of Gibbs free energy, at 298.15 K. According to these results, this path is not expected to significantly contribute to the overall OH + MMC reaction.

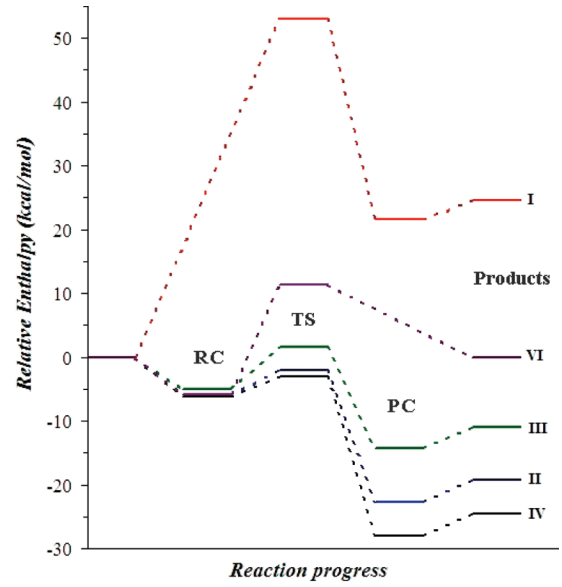

Figure 5. Energy profiles of the different studied paths of reaction.

The energy profiles of all of the computed paths of reactions in terms of enthalpy and relative to the isolated reactants are comparatively shown in Figure 5. The Gibbs free energy and enthalpy values are provided as Supporting Information (Table SI). As Figure 5 shows, the lower profiles correspond to H abstraction paths, which suggest that they are those contributing the most to the environmental loss process of MMC, when OH radicals are present.

Table 1. Calculated Rate Constants[a]

T (K)	k_I	k_{II}	k_{III}	k_{IV}	k_{VI}
260	6.33×10^{-29}	1.68×10^{-13}	8.03×10^{-16}	4.09×10^{-12}	4.08×10^{-25}
280	1.32×10^{-26}	1.66×10^{-13}	8.80×10^{-16}	4.05×10^{-12}	2.29×10^{-24}
298.15	1.20×10^{-24}	1.75×10^{-13}	9.63×10^{-16}	3.99×10^{-12}	8.97×10^{-24}
300	1.86×10^{-24}	1.79×10^{-13}	9.72×10^{-16}	3.98×10^{-12}	1.02×10^{-23}
320	1.84×10^{-22}	2.25×10^{-13}	1.08×10^{-15}	3.89×10^{-12}	3.81×10^{-23}
340	1.28×10^{-20}	2.73×10^{-13}	1.20×10^{-15}	3.80×10^{-12}	1.22×10^{-22}
360	6.34×10^{-19}	3.24×10^{-13}	1.35×10^{-15}	3.69×10^{-12}	3.46×10^{-22}
380	2.26×10^{-17}	3.74×10^{-13}	1.51×10^{-15}	3.59×10^{-12}	8.80×10^{-22}
400	5.98×10^{-16}	4.24×10^{-13}	1.69×10^{-15}	3.51×10^{-12}	2.05×10^{-21}

[a] I: TST, s^{-1}. II, III, and IV: IVTST-M-8/10, cm^3 $molecule^{-1}$ s^{-1}. VI: TST, cm^3 $molecule^{-1}$ s^{-1}.

Kinetics and Branching Ratios. As it is shown in Figure 5, paths I and VI have barriers that are higher than 10 kcal/mol. Accordingly, their kinetic study was performed only by conventional transition state theory (TST). For H abstraction paths, on the other hand, the IVTST-M-*H*/*G* was used.

For the calculation of the rate constants (k), a complex mechanism has been proposed for many radical−molecule reactions.[28−32,34] It involves a fast pre-equilibrium between the isolated reactants and a reactants complex (RC), followed by an irreversible step leading to the formation of products. In a classical treatment, the calculation of the overall rate coefficient depends only on the properties of reactants and transition states, and it can be shown that the RC energy and partition function cancels out in the rate constant expression.[35] However, when there is a possibility of quantum mechanical tunneling, the existence of the reactant complex might change the tunneling factor. In the present work, the H abstraction reactions have two reactants and two products, and weak bonded complexes have been found in both reactant and product channels. They have been explicitly considered in the potential surface and included in the IVTST-M calculations.

Because accurate rate constant calculations require proper evaluation of the partition functions (Q), the hindered rotor approximation has been used to correct the Q's corresponding to internal rotations with torsional barriers comparable to RT. Direct inspection of the low-frequency modes of the studied stationary points indicates that there are several modes that correspond to hindered rotations. These modes should be treated as hindered rotors instead as vibrations.[36] To make this correction, these modes were removed from the vibrational partition function of the corresponding specie and replaced with the hindered rotor partition function (Q^{HR}). In our calculations, we have adopted the analytical approximation to Q^{HR} for a one-dimensional hindered internal rotation proposed by Ayala and Schlegel.[37]

The values of the calculated rate constants are reported in Table 1. Those corresponding to paths II, III, and IV were obtained using the IVTST-M-8/10 methodology and SCT tunneling. Path I was found to be the slowest one, in the temperature range 260−400 K, despite the fact that its rate constant was calculated using TST, which represents an upper limit of CVT. Its rate constant shows a marked increase with temperature. Therefore, even though at temperatures relevant to atmospheric chemistry this path can be neglected, for higher temperatures it might become significant. The Arrhenius expression for this range was found to be $6.25 \times 10^8 \exp(-4421/RT)$. However, because this decomposition pathway was experimentally studied in the 370−422 K range, our data in an equivalent range were also fitted to an Arrhenius plot, and the activation energy was found to be 48.77 kcal/mol, in excellent agreement with the experimental value (48.06 kcal/mol).[9] This agreement supports the reliability of the calculated values.

Table 2. Branching Ratios (Γ), in Percentage, Corresponding to All of the Viable Paths (IVTST-M-8/10)

T (K)	Γ_I	Γ_{II}	Γ_{III}	Γ_{IV}	Γ_{VI}
260	1.7×10^{-21}	3.96	0.02	96.03	9.6×10^{-12}
280	3.6×10^{-19}	3.93	0.02	96.05	5.4×10^{-11}
298.15	3.3×10^{-17}	4.19	0.02	95.79	2.2×10^{-10}
300	5.1×10^{-17}	4.29	0.02	95.68	2.5×10^{-10}
320	5.1×10^{-15}	5.47	0.03	94.51	9.3×10^{-10}
340	3.6×10^{-13}	6.71	0.03	93.26	3.0×10^{-09}
360	1.8×10^{-11}	8.06	0.03	91.91	8.6×10^{-09}
380	6.6×10^{-10}	9.42	0.04	90.54	2.2×10^{-08}
400	1.7×10^{-08}	10.77	0.04	89.19	5.2×10^{-08}

The addition to the C atom in the carbonyl group was also found to be several orders of magnitude slower than those corresponding to H abstraction paths. Accordingly, it seems that the MMC reaction with OH radicals occurs mainly by H transfers from the carbamate to the radical. The largest rate constant was found for path IV in the whole studied temperature range, followed by that of path II. The H abstraction from the NH group was found to be the slowest among the H abstraction paths.

To quantify the contributions of the different paths to the overall rate coefficient, the corresponding branching ratios (Γ) expressed as percent were calculated and are reported in Table 2. They have been computed for a 24 h daytime average concentration of OH equal to 8.7×10^5 molecule cm^{-3}.[38] According to the values in this table, the only channels significantly contributing to the MMC + OH gas-phase reaction are the H abstractions from the methyl groups (paths II and IV). The contributions of all other paths together are less than 0.3% and can be neglected, at least within the studied temperature range. The contribution of H abstraction paths from amino groups to the overall rate coefficient in their reactions with OH radicals has been found to be up to 20%.[39] However, in this case, the contribution of path III was found to be negligible. This can be rationalized in terms of the structural differences between amine and −N(H)-C(O)O− moieties. The N atom in amines is bonded to alkyl groups, which have electron-donor character, helping to cope with the charge deficiency in the forming N radical center.

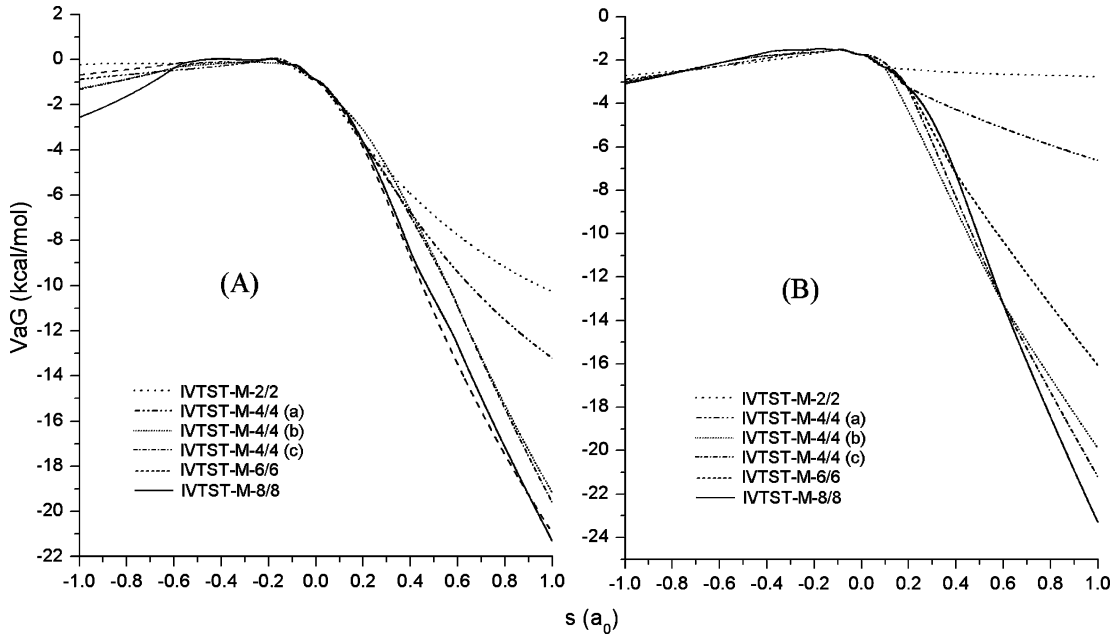

Figure 6. VaG(s), relative to isolated reactants, using the MEP generated by IVTST-M-2/2, IVTST-M-4/4 [H and G at $s = \pm 0.1$ and $\pm 0.2a_0$ (a); ± 0.1 and $\pm 0.6a_0$ (b); ± 0.2 and $\pm 0.6a_0$ (c)], IVTST-M-6/6, and IVTSTM-8/8. (A) Path II, (B) path IV.

The N atoms in carbamates, on the other hand, are bonded to −C(O)O− fragments with high electron-withdrawing character. Therefore, its presence deactivates the H abstraction from the NH site.

Path IV was found to contribute the most to the overall rate coefficient, from 96% at 260 K to 89.2% at 400 K, while the contribution of path II goes from ∼4% to 10.8%. These findings are in agreement with the information inferred from the work by Kwok et al.[10] that the contribution of H abstraction from the alkyl group on the N side should be larger than that of the alkyl group on the ester side, provided that similar alkyl groups are bonded to the N and the O atoms in carbamates. The presence of the electron-withdrawing −C(O)O− fragment in the vicinity of the methyl group, involved in the H abstraction, reduces the feasibility of such process, as compared to that of the equivalent alkyl group at the N side. In addition, it seems worthwhile to call attention to the fact that moving upward in the troposphere implies a lowering in temperatures; therefore, path II is expected to become less and less important as the altitude increases.

After the main paths of reaction were identified, the performance of different levels of dynamic calculations IVTST-M-*H*/*G* has been tested for them. Figure 6 shows the obtained ground-state vibrationally adiabatic potential energy paths defined as:

$$V_a^G(s) = V_{MEP}(s) + E_{int}(s) \quad (1)$$

where $V_{MEP}(s)$ is the classical potential energy path, and $E_{int}(s)$ is the local zero-point energy (ZPE) at s. Three different curves are shown within the IVTST-M-4/4 scheme. They differ in the s values at which the four nonstationary points have been chosen: (a) in the vicinity of the transition state, $s = \pm 0.1$ and $\pm 0.2a_0$; (b) two points in the vicinity ($s = \pm 0.1a_0$) and two points away ($s = \pm 0.6a_0$) from the TS; and (c) at the points where the IRC shows the maximum curvature. For path IV, the curvature on the product side shows one very sharp change at $s = +0.6a_0$, while the reactant side shows modest changes at $s = -0.2$ and $-0.6a_0$. For path II, there is also a sharp curvature change on the product side, this time at $s = +0.4a_0$, while on the reactant side the curvature change is almost negligible. As Figure 6 shows, the largest discrepancies among the different IVTST-M-*H*/*G* schemes appear on the product side and are more significant at large distances from the saddle points. For the main path of reaction IV, there is an excellent coincidence among the surfaces on the reactant side. The selection of the nonstationary points plays an important role in the shape of the interpolated VaG curve. If they are chosen taking into account the curvature of the MEP, the adiabatic surface obtained at IVTST-M-4/4 is very close to the IVTST-M-8/8 one. This is an interesting result because, depending on the size of the studied system, such a reduction in the number of computed Hessians might represent a significant saving in the computational cost. In the present work, the main paths of reaction show no tunneling effects; therefore, only slight differences are expected among the calculated rate constants as a consequence of the *H*/*G* choice. However, because the shape of the VaG curve plays a critical role in tunneling calculations, the above-discussed results show that a careful selection of the nonstationary points used for the interpolation is essential when tunneling becomes significant and a modest IVTST-M-*H*/*G* scheme is used. From this point on, and based on the results shown in Figure 6, the results reported with IVTST-M-4/4 refer to those obtained including the nonstationary points at the s values of maximum curvature. The absence of tunneling effects is caused by the low and broad barriers found in these cases.

Computing the overall rate coefficient as the sum of k_{II} and k_{IV}, which are the only paths significantly contributing to it, the nine tested IVTST-M schemes are very close and within the experimental error (Table 3), with the exception

Table 3. Overall Rate Coefficients at 298 K (k^{298}, in cm^3 molecule^{-1} s^{-1}), Arrhenius Activation Energies (*Ea*, in kcal/mol), Arrhenius Pre-exponential Factor (*A*, in cm^3 molecule^{-1} s^{-1}), and Reaction Coordinate of the Variational Transition States for Paths II and IV (*s*, in bohr)

	$k^{298} \times 10^{12}$	*Ea*	$A \times 10^{12}$	$s_{II}^{IVTST-M}$	$s_{IV}^{IVTST-M}$
IVTST-M-2/2	4.53	−0.16	3.46	−0.1872	−0.0989
IVTST-M-2/4	4.23	−0.06	3.83	−0.0832	−0.0836
IVTST-M-4/4	4.44	−0.15	3.47	−0.1758	−0.0900
IVTST-M-4/6	4.17	−0.10	3.50	−0.1921	−0.1837
IVTST-M-4/8	4.17	−0.11	3.45	−0.1919	−0.1831
IVTST-M-4/10	4.18	−0.11	3.48	−0.1955	−0.1835
IVTST-M-6/6	4.18	−0.09	3.57	−0.1888	−0.1798
IVTST-M-6/8	4.29	−0.12	3.47	−0.2030	−0.1904
IVTST-M-8/10	4.17	−0.12	3.40	−0.4855	−0.1812
exp[10]	4.30 ± 1.2				

of that obtained within the IVTST-M 2/2 scheme. However, even in this case, the calculated rate constant is only 1.05 times larger than the experimental one, which represents about 5.5% error. The Arrhenius activation energies were found to be slightly negative, varying from −0.06 to −0.16 kcal/mol. On the basis of the results from the largest values of *H* and *G*, a value of (−0.10 ± 0.02) kcal/mol is proposed for the activation energy. All of the calculated pre-exponential factors show very similar values, in the range (3.40−3.83) × 10^{-12} cm^3 molecule^{-1} s^{-1}. The variational transition state was found to be located on the reactant side for all of the tested IVTST-M-*H*/*G* schemes.

The values of the overall rate coefficients obtained using the IVTST-M-8/10 at the different studied temperatures together with the ratios of the values obtained within the other tested schemes with respect to IVTST-M-8/10 are reported in Table SII, as Supporting Information. The values of these ratios are all very close to unity, confirming the consistency of the IVTST-M-*H*/*G* methodology. As expected, the largest ratios correspond to the lowest *H* values (*H* = 2). The variational effects defined as k^{TST}/k^{ICVT} allow quantifying the overestimation of the TST rate constants, that is, the importance of using VTST. They were found to be rather small for path II: smaller than 1.8 regardless of the temperature and the *H*/*G* combination (Table SIII). For path IV, the variational effects are significantly larger, with values up to 7.02. Because both paths represent OH hydrogen abstractions from methyl groups, it seems that the atom directly bonded to the methyl group is responsible for the difference in the variational effects. Apparently, the presence of the O atom in the vicinity of the reaction site influences the thermal correction to Gibbs free energy to a larger extension than does the presence of an N atom, probably due to the relative higher electronegativity of the oxygen. It might lead to a tighter transition state with a larger loss of entropy, relative to the reactants. The variation of the k^{TST}/k^{ICVT} ratio was found to be almost independent of the IVTST-M-*H*/*G* level, for all of the tested *H*/*G* combinations, with the exception of IVTST-M-2/4 that led to variational effects for path II that are about one-half the magnitude of those obtained for any other tested *H*/*G* combination. In all cases, and for both paths, the variational effects were found to decrease as the temperature rises, which is consisted with the results reported for the OH hydrogen abstraction from methane.[21]

In the original paper presenting IVTST-M-*H*/*G*, it was established that using $H \geq 6$ is enough to obtain good results.[21] Considering the data from Tables 3, SII, and SIII all together, it seems that providing Hessians and gradients for as few as four nonstationary points along the MEP is sufficient to achieve an excellent accuracy, provided that the data for these few points are obtained at high-quality levels of theory and that they are chosen taking the curvature of the surface into account. In fact, it seems that the interpolation by mapping works efficiently even when only four Hessians and four gradients are explicitly provided, at least for H abstraction reactions from alkyl groups.

Conclusions

Different paths of reaction have been modeled, at high level of theory, accounting for the possible atmospheric fate of methyl *N*-methylcarbamate. It has been shown that its unimolecular gas-phase decomposition yielding methyl isocyanate and methanol is negligible, especially at atmospheric temperatures and when OH radicals are present. The addition of the OH radical to the N atom in the −N(H)C(O)O− moiety has been ruled out as well. The OH hydrogen abstractions from the methyl groups in MMC account for almost the 100% of the MMC + OH gas-phase reaction. The H abstraction from the methyl group at the N side was found to be the main path of reaction, with contributions to the overall reaction from 96% at 260 K to 89.2% at 400 K. Hydrogen abstractions from the other methyl group were identified as a secondary, but significant path, with contributions from ∼4% to 10.8%. The Arrhenius activation energy, in the temperature range 260−400 K, was found to be close to zero, but slightly negative. The proposed value is (−0.10 ± 0.02) kcal/mol. The excellent agreement with the scarce experimental data available supports the reliability of the data reported here for the first time. Different IVTST-M-*H*/*G* schemes were tested for dynamic calculations. The high efficiency of the Interpolated Variational Transition-State Theory by Mapping, when only a very small number of points along the reaction path are explicitly included in the calculations, has been proven. According to our results, providing the Hessians and gradients for as few as four nonstationary points along the MEP is sufficient to achieve an excellent accuracy, provided that the data for these few points were obtained from high-quality levels of theory, at least for H abstraction reactions from alkyl groups. It should be noticed, however, that for reactions with significant tunneling the selection of the nonstationary points plays an important role in the quality of the interpolated MEP. For better results, those points at *s* values corresponding to the maximum curvature should be included.

Acknowledgment. We thank Prof. Donald G. Truhlar for providing the POLYRATE 9.1 program and Prof. J. R. Alvarez-Idaboy for helpful discussions. A.G. also thanks professors D. G. Truhlar and J. Zheng for their valuable help and advice on dynamic calculations, and Laboratorio de

Visualización y Cómputo Paralelo at UAM - Iztapalapa for the access to its computer facilities. The work in Guanajuato was funded by Conacyt (Grant 57892). C.Z.-O. acknowledges CONACyT for the Master fellowship.

Supporting Information Available: Enthalpies and Gibbs free energies of the stationary points, relative to the isolated reactants. Overall IVTST-M-8/10 rate coefficients at the different studied temperatures and ratios IVTST-M-*H*/*G*/IVTST-M-8/10. Variational effects k^{TST}/k^{IVTST} within the 260−400 K temperature range for paths II and IV, from all tested IVTST-M-*H*/*G* methods. This material is available free of charge via the Internet at http://pubs.acs.org.

References

(1) Dibenedetto, A.; Aresta, M.; Fragale, C.; Narracci, M. *Green Chem.* **2002**, *4*, 439.

(2) Gupta, S. P.; Shivarkar, A. B.; Chaudhari, R. V. *J. Chem. Soc., Chem. Commun.* **2001**, 2620.

(3) Motolcsy, G.; Nadasy, M.; Andriska, V. *Pesticide Chemistry*; Academiai Kiado: Budapest, 1988; p 90.

(4) Thompson, A. *Pesticide Outlook* **2002**, *13*, 84.

(5) Lawrence, M.; Klein, D. L.; Nemotho, P. *Bioorg. Med. Chem. Lett.* **1997**, *7*, 157.

(6) Greene, W. T.; Wuts, P. G. M. *Protective Groups in Organic Synthesis*, 2nd ed.; Wiley: New York, 1991; pp 327 and 403.

(7) Atkinson, R. Atmospheric Transformations of Automotive Emissions. In *Air Pollution, the Automobile, and Public Health*; Watson, A. Y., Bates, R. R., Kennedy, D., Eds.; National Academy Press: Washington, DC, 1988; pp 99−132.

(8) Atkinson, R. J. *Phys. Chem. Ref. Data* **1994**, 1, Monograph 2.

(9) Daly, N. J.; Ziolkowski, F. *Aust. J. Chem.* **1972**, *25*, 1453.

(10) Kwok, E. S. C.; Aschmann, S.; Atkinson, R. *Environ. Sci. Technol.* **1996**, *30*, 329.

(11) Kwok, E. S. C.; Atkinson, R.; Arey, J. *Environ. Sci. Technol.* **1992**, *26*, 1798.

(12) Seakins, P. W. *Annu. Rep. Prog. Chem., Sect. C: Phys. Chem.* **2007**, *103*, 173.

(13) Butkovskaya, N. I.; Kukui, A.; Le Bras, G. *J. Phys. Chem. A* **2004**, *108*, 1160.

(14) Butkovskaya, N. I.; Setser, D. W. *J. Phys. Chem. A* **1999**, *103*, 6921.

(15) Butkovskaya, N. I.; Kukui, A.; Pouvesle, N.; Le Bras, G. *J. Phys. Chem. A* **2004**, *108*, 7021.

(16) Frisch, M. J.; Trucks, G. W.; Schlegel, H. B.; Scuseria, G. E.; Robb, M. A.; Cheeseman, J. R.; Montgomery, J. A., Jr.; Vreven, T.; Kudin, K. N.; Burant, J. C.; Millam, J. M.; Iyengar, S. S.; Tomasi, J.; Barone, V.; Mennucci, B.; Cossi, M.; Scalmani, G.; Rega, N.; Petersson, G. A.; Nakatsuji, H.; Hada, M.; Ehara, M.; Toyota, K.; Fukuda, R.; Hasegawa, J.; Ishida, M.; Nakajima, T.; Honda, Y.; Kitao, O.; Nakai, H.; Klene, M.; Li, X.; Knox, J. E.; Hratchian, H. P.; Cross, J. B.; Bakken, V.; Adamo, C.; Jaramillo, J.; Gomperts, R.; Stratmann, R. E.; Yazyev, O.; Austin, A. J.; Cammi, R.; Pomelli, C.; Ochterski, J. W.; Ayala, P. Y.; Morokuma, K.; Voth, G. A.; Salvador, P.; Dannenberg, J. J.; Zakrzewski, V. G.; Dapprich, S.; Daniels, A. D.; Strain, M. C.; Farkas, O.; Malick, D. K.; Rabuck, A. D.; Raghavachari, K.; Foresman, J. B.; Ortiz, J. V.; Cui, Q.; Baboul, A. G.; Clifford, S.; Cioslowski, J.; Stefanov, B. B.; Liu, G.; Liashenko, A.; Piskorz, P.; Komaromi, I.; Martin, R. L.; Fox, D. J.; Keith, T.; Al-Laham, M. A.; Peng, C. Y.; Nanayakkara, A.; Challacombe, M.; Gill, P. M. W.; Johnson, B.; Chen, W.; Wong, M. W.; Gonzalez, C.; Pople, J. A. *Gaussian 03*, revision E.01; Gaussian, Inc.: Wallingford, CT, 2004.

(17) Montgomery, J. A.; Frisch, M. J.; Ochterski, J. W.; Petersson, G. A. *J. Chem. Phys.* **1999**, *110*, 2822.

(18) (a) Nyden, M. R.; Petersson, G. A. *J. Chem. Phys.* **1981**, *75*, 1843. (b) Al-Laham, M. A.; Petersson, G. A. *J. Chem. Phys.* **1991**, *94*, 6081. (c) Petersson, G. A.; Tensfeldt, T. G.; Montgomery, J. A. *J. Chem. Phys.* **1991**, *94*, 6091. (d) Petersson, G. A.; Malick, D. K.; Wilson, W. G.; Ochterski, J. W.; Montgomery, J. A.; Frisch, M. J. *J. Chem. Phys.* **1998**, *109*, 10570. (e) Montgomery, J. A.; Frisch, M. J.; Ochterski, J. W.; Petersson, G. A. *J. Chem. Phys.* **2000**, *112*, 6532.

(19) Gonzalez, C.; Schlegel, H. B. *J. Phys. Chem.* **1990**, *94*, 5523.

(20) (a) Gonzalez, C.; Schlegel, H. B. *J. Chem. Phys.* **1989**, *90*, 2154. (b) Gonzalez, C.; Schlegel, H. B. *J. Phys. Chem.* **1990**, *94*, 5523.

(21) Corchado, J. C.; Coitiño, E. L.; Chuang, Y.-Y.; Fast, P. L.; Truhlar, D. G. *J. Phys. Chem. A* **1998**, *102*, 2424.

(22) Corchado, J. C.; Chuang, Y.-Y.; Fast, P. L.; Villà, J.; Hu, W.-P.; Liu, Y.-P.; Lynch, G. C.; Nguyen, K. A.; Jackels, C. F.; Melissas, V. S.; Lynch, B. J.; Rossi, I.; Coitiño, E. L.; Fernandez-Ramos, A.; Pu, J.; Albu, T. V.; Steckler, R.; Garrett, B. C.; Isaacson, A. D.; Truhlar, D. G. *POLYRATE-version 9.1*; University of Minnesota: Minneapolis, 2002.

(23) (a) Isaacson, A. D.; Truhlar, D. G. *J. Chem. Phys.* **1982**, *76*, 1380. (b) Truhlar, D. G.; Garrett, B. C. *Annu. Rev. Phys. Chem.* **1984**, *35*, 159. (c) Chuang, Y.-Y.; Cramer, C. J.; Truhlar, D. G. *Int. J. Quantum Chem.* **1998**, *70*, 887.

(24) (a) Garrett, B. C.; Truhlar, D. G.; Grev, R. S.; Magnuson, A. W. *J. Phys. Chem.* **1980**, *84*, 1730. (b) Truhlar, D. G.; Garrett, B. C. *Annu. Rev. Phys. Chem.* **1984**, *35*, 159. (c) Truhlar, D. G.; Liu, Y.-P.; Schenter, G. K.; Garrett, B. C. *J. Phys. Chem.* **1994**, *98*, 8396.

(25) Chuang, Y.-Y.; Truhlar, D. G. *J. Phys. Chem. A* **1998**, *102*, 242.

(26) (a) Eyring, H. *J. Chem. Phys.* **1935**, *3*, 107. (b) Truhlar, D. G.; Hase, W. L.; Hynes, J. T. *J. Phys. Chem.* **1983**, *87*, 2664.

(27) Eckart, C. *Phys. Rev.* **1930**, *35*, 1303.

(28) Singleton, D. L.; Cvetanovic, R. J. *J. Am. Chem. Soc.* **1976**, *98*, 6812.

(29) Mora-Diez, N.; Alvarez-Idaboy, J. R.; Boyd R, J. *J. Phys. Chem. A* **2001**, *105*, 9034.

(30) Alvarez-Idaboy, J. R.; Mora-Diez, N.; Boyd R, J.; Vivier-Bunge, A. *J. Am. Chem. Soc.* **2001**, *123*, 2018.

(31) Galano, A.; Alvarez-Idaboy, J. R.; Ruiz-Santoyo, M. E.; Vivier-Bunge, A. *ChemPhysChem* **2004**, *5*, 1379.

(32) Francisco-Marquez, M.; Alvarez-Idaboy, J. R.; Galano, A.; Vivier-Bunge, A. *Phys. Chem. Chem. Phys.* **2003**, *5*, 1392.

(33) Galano, A.; Alvarez-Idaboy, J. R.; Ruiz-Santoyo, M. E.; Vivier-Bunge, A. *J. Phys. Chem. A* **2005**, *109*, 169.

(34) Galano, A.; Alvarez-Idaboy, J. R. Atmospheric Reactions of Oxygenated Compounds + OH radicals: Role of Hydrogen-Bonded Intermediates and Transition States. In *Advances in Quantum Chemistry: Applications of Quantum Chemistry*

to the Atmosphere; Goodsite, M. E., Johnson, M. S., Eds.; Elsevier Pub.: Amsterdam, 2008; Chapter 12, pp 245−274.

(35) Alvarez-Idaboy, J. R.; Cruz-Torres, A.; Galano, A.; Ruiz-Santoyo, M. E. *J. Phys. Chem. A* **2004**, *108*, 2740.

(36) Jacox, M. E. *Vibrational and Electronic Energy Levels of Polyatomic Transient Molecules*; NIST: Gaithersburg, MD, 1998; Vol. 69, p 945.

(37) Ayala, P. Y.; Schlegel, H. B. *J. Chem. Phys.* **1998**, *108*, 2314.

(38) Prinn, R.; Cunnold, D.; Simmonds, P.; Alyea, F.; Boldi, R.; Crawford, A.; Fraser, P.; Gutzler, D.; Hartley, D.; Rosen, R.; Rasmussen, R. *J. Geophys. Res.* **1992**, *97*, 2445.

(39) Galano, A.; Alvarez-Idaboy, J. R. *J. Chem. Theory Comput.* **2008**, *4*, 322.

CT9000679